

1 **Estimating the Top Altitude of Optically Thick Ice Clouds from Thermal Infrared Satellite**
2 **Observations Using CALIPSO Data**

3

4 Patrick Minnis¹, Chris R. Yost², Sunny Sun-Mack², and Yan Chen²

5

6

7 ¹NASA Langley Research Center, Hampton, VA, USA

8 ²Science Systems and Applications, Inc., Hampton, VA, USA

9

10

11

12

13

14

15

16

17

Submitted to *Geophysical Research Letters*

18

March 2008

19

19 **Abstract**

20 A parameterization to estimate the true cloud-top altitude Z_{top} from the infrared effective
21 radiating height Z_{eff} for optically thick ice clouds is developed using cloud altitude data taken by
22 the Cloud-Aerosol Lidar and Infrared Pathfinder Satellite Observations (CALIPSO) and the
23 *Aqua* Moderate-Resolution Imaging Spectroradiometer (MODIS) during April 2007. The mean
24 difference between CALIPSO Z_{top} and MODIS Z_{eff} is 1.58 ± 1.26 km for even days. A simple
25 linear fit between Z_{top} and Z_{eff} removes the bias. The resulting equation applied to odd-day data
26 yields a difference of 0.03 ± 1.21 km indicating general applicability. The instantaneous
27 uncertainties are likely due to cloud inhomogeneities, to errors in the temperature profiles and,
28 primarily, to natural variations in cloud ice water content. The latter was estimated to be, on
29 average, $\sim 0.15 \text{ gm}^{-3}$ in the top portions of the observed clouds. The method should be applicable
30 to any infrared-based effective height for thick ice clouds.

31

31 **1. Introduction**

32 Spectral bands in the infrared (IR) atmospheric window (10-12 μm) are routinely used to
33 estimate cloud top heights from passive satellite sensors [e.g., *Rossow and Schiffer, 1999; Minnis*
34 *et al., 1995*]. Radiation in this spectral range is relatively transparent to the atmosphere above
35 the cloud, and the observed 11- μm brightness temperature T_{11} can be matched to local
36 temperature soundings to find the cloud height. Although it is recognized that the effective
37 radiating temperature of optically thin cirrus clouds corresponds to some level, sometimes far,
38 below cloud top, it is commonly assumed that optically thick, particularly deep convective,
39 clouds have sharp boundaries and optically thick edges. They are treated as blackbodies for most
40 purposes, and so T_{11} is assumed to be equivalent to the temperature of the true cloud top plus a
41 small correction for atmospheric absorption and cloud particle scattering. Recent research has
42 demonstrated, however, that even deep convective clouds typically do not have such sharply
43 defined boundaries in the IR spectrum. For example, *Sherwood et al. [2004]* found that cloud
44 tops derived from the eighth Geostationary Operational Environmental Satellite (GOES-8) were
45 1-2 km below the tops of convective clouds detected by lidar data collected over Florida. Those
46 and other results require the development of new approaches to interpret the infrared brightness
47 temperatures of optically thick clouds. Measurements from active sensors combined with passive
48 infrared radiances are needed to address this outstanding problem in cloud remote sensing.

49 Until recently, active remote sensing of optically thick clouds has been extremely limited.
50 Ground-based radars and lidars profile the atmosphere continuously, but observe only one
51 location. They are also unlikely to detect the physical tops of optically thick ice clouds because
52 lidars can only penetrate to optical depths of no greater than about 3 into the cloud and cloud
53 radars often have no returns from the smaller ice crystals common at the tops of such clouds.

54 Active sensors aboard aircraft can sample a larger area during field campaigns and can outline
55 the tops of the clouds, but they collect data for only a few days over the duration of a given
56 experiment. With the 2006 launch of the Cloud-Aerosol Lidar and Infrared Pathfinder Satellite
57 Observations (CALIPSO) satellite into orbit behind the *Aqua* satellite in the A-Train, coincident
58 and nearly simultaneous global lidar and infrared radiance measurements are now available. This
59 study uses the measurements from CALIPSO and the *Aqua* Moderate-Resolution Imaging
60 Spectroradiometer (MODIS) to develop a new method to estimate the physical top of optically
61 thick ice clouds from passive infrared imager data.

62

63 **2. Data and Methodology**

64 Like *Aqua*, CALIPSO follows a Sun-synchronous orbit with an approximately 1330-LT
65 equatorial crossing time roughly 90 s behind *Aqua*. Because the CALIPSO orbit is offset by
66 between 7 and 18° to the east of *Aqua*, the *Aqua* sensors typically observe the CALIPSO ground
67 track at viewing zenith angles VZA between 9 and 19°. The primary instrument on CALIPSO is
68 the Cloud Aerosol Lidar with Orthogonal Polarization (CALIOP), which has 532 and 1064-nm
69 channels for profiling cloud and aerosol layers [Winker *et al.*, 2007]. The CALIOP footprints
70 have a nominal diameter of 70 m and are sampled every 330 m. This instrument allows the
71 characterization of cloud vertical structure all over the globe with vertical resolutions of up to 30
72 m. The CALIPSO data used here are the April 2007 Version 1.21 1/3 km cloud height products
73 [Vaughan *et al.*, 2004].

74 Cloud properties derived from 1-km *Aqua* MODIS radiances using the Clouds and the
75 Earth's Radiant Energy System (CERES) project cloud retrieval algorithms [Minnis *et al.*, 2006]
76 were matched with CALIOP data as described by Sun-Mack *et al.* [2007]. The CERES cloud

77 properties are determined from the radiances using updated versions of the daytime Visible
78 Infrared Solar-Infrared Split Window Technique (VISST) and the nighttime Solar-infrared
79 Infrared Split-window Technique (SIST) [Minnis *et al.*, 1995]. The products include cloud
80 temperature, height, thermodynamic phase, optical depth, and other cloud properties.

81 The VISST/SIST first characterizes a cloud in terms of an effective radiating temperature
82 T_{eff} , which corresponds to a height somewhere within the cloud z_{eff} [e.g., Minnis *et al.*, 1990].
83 For clouds above 500 hPa, the value of z_{eff} is determined by matching T_{eff} to a local atmospheric
84 temperature sounding and taking the corresponding height to be z_{eff} . For optically thin ice clouds,
85 an empirical correction is applied to estimate the true cloud top temperature T_{top} based on the
86 cloud emissivity [Minnis *et al.*, 1990]. The cloud-top altitude Z_{top} for those clouds is the lowest
87 level in the sounding corresponding to T_{eff} . Deep convective clouds and other optically thick
88 clouds are assumed to have sharp, optically thick boundaries and therefore, most of the infrared
89 radiation reaching the satellite sensor is emitted by the uppermost part of the cloud. In these
90 optically thick cases, it is assumed in both VISST and SIST that T_{eff} is equivalent to T_{top} and z_{top}
91 = z_{eff} . The VISST accounts for the effects of infrared scattering so that for these clouds, T_{eff} will
92 be slightly greater than T_{II} .

93 Matched VISST and CALIPSO data from every even day during April 2007 were
94 selected to develop a relationship between the effective and physical cloud-top heights of
95 optically thick ice clouds. In the analysis, clouds with effective emittance exceeding 0.98 (visible
96 optical depth $\tau > 8$) are considered to be optically thick. Polar clouds (latitudes $> 60^\circ$) were
97 excluded from the analysis to avoid mischaracterizing clouds over sea ice and snow. After
98 developing the method to estimate cloud-top height for optically thick ice clouds, it is tested
99 using the remaining (odd days) April 2007 MODIS-CALIPSO non-polar matched data.

100 3. Cloud-Top Height Correction

101 Figure 1 shows a profile of CALIOP backscatter intensities (Figure 1a) and scene
102 classifications for a 1-h segment of a 27 April 2007 CALIPSO orbit centered at 1030 UTC. The
103 orbital segment began in darkness over North America, crossed the Pacific, passed over
104 Antarctica into daylight, and ended in the Indian Ocean. The scene classifications in Figure 1b,
105 which show cloud and aerosol locations, are overlaid with black dots corresponding to the
106 CERES-MODIS values of Z_{top} for optically thick single-layer ice clouds. In general, the CERES-
107 MODIS cloud tops are 1-2 km below the top indicated by CALISPO.

108 These cloud-top height pairs and those for all even days during April 2007 are plotted in
109 Figure 2 as density scatter plots with linear regression fits. In Figure 2a, the average difference
110 between the 15,367 CALIPSO cloud top heights Z_{topCAL} and their Z_{eff} counterparts increases
111 slightly with increasing altitude. The mean difference, $Z_{eff} - Z_{topCAL}$, is -1.58 ± 1.26 km. The
112 linear regression fit plotted over the data is

113

$$114 \quad Z_{top} = 1.094 Z_{eff} + 0.751 \text{ km.} \quad (1)$$

115

116 It yields a squared linear correlation coefficient $R^2 = 0.89$. According to the linear fit, the
117 difference ΔZ between Z_{top} and Z_{eff} rises from ~ 1.25 km for $Z_{eff} = 5$ km up to more than 2 km for
118 $Z_{eff} > 14$ km.

119 Applying Eq (1) to the Z_{eff} values in Figure 1b yields the new values in Figure 1c that, in
120 general, are very close to the corresponding CALIPSO cloud tops. Figure 2b compares the
121 15,170 values of Z_{topCAL} and Z_{top} computed with Eq (1) for all April 2007 odd-day data. The data
122 corresponding to $Z_{topCAL} > 3$ km are centered along the line of agreement, while lower clouds are

123 overestimated with the correction to the MODIS data. That correction yields a mean difference
124 of -0.03 ± 1.21 km and the resulting data more correlated than the odd day data, having $R^2 =$
125 0.91. This empirical correction effectively eliminates the bias and slightly reduces the random
126 error in the estimated Z_{top} . The correction is robust in that it applies well to two independent
127 datasets. The Z_{top} estimates were not constrained to be below the tropopause.

128 For $Z_{eff} < 3$ km, the data tend to be centered on the line of agreement in Figure 2a
129 indicating that no correction is needed. The correction results in unphysical values and should
130 not be applied. This overestimation could be the result of uncertainties in the atmospheric profile
131 of temperature in the lower layers due the occurrence of sharp inversions (e.g., *Dong et al.*
132 [2008]) or due to the misclassification of supercooled liquid water or mixed-phase clouds as ice
133 clouds by the *Aqua* algorithm. The basic assumption that the correction is for ice clouds would
134 be violated for those and other low-level pixels. The tops of water clouds are unlikely to be more
135 than a few hundred meters above Z_{eff} [e.g., *Dong et al.*, 2008]. For the lower level clouds, it is
136 important to first obtain a better estimate of Z_{eff} and a more accurate phase classification before
137 applying a correction to obtain Z_{top} . That effort is beyond the scope of this paper.

138 To minimize the impact of low-altitude temperature and phase uncertainties in the
139 retrievals, the regression was also performed using the data (13,046 samples) only for ice clouds
140 with effective pressures, $p_{eff} < 500$ hPa. The resulting fit is

141

$$142 \quad Z_{top} = 1.041 Z_{eff} + 1.32 \text{ km.} \quad (2)$$

143

144 Applying Eq (2) to the odd-day clouds having $p_{eff} < 500$ hPa yields an average difference of -
145 0.08 ± 1.15 km. This difference is nearly the same as the average difference of -0.13 ± 1.14 km

146 that would be obtained by applying Es (1) to the same dataset. If Eq (2) is used to estimate Z_{top}
 147 for all of the odd-day data, the mean difference is 0.07 ± 1.24 km. It does not make much
 148 difference which fit is used, the results are essentially the same. The 500-hPa cutoff for applying
 149 either fit is somewhat arbitrary, but it effectively eliminates the lower cloud heights that would
 150 be overestimated by estimating Z_{top} from Z_{eff} with either correction.

151

152 **4. Discussion**

153 Although the empirical correction minimizes the bias, the instantaneous differences
 154 remain relatively large. Those differences can mainly be attributed to uncertainties in the
 155 temperature profiles used to convert temperature to altitude, spatial mismatches in the data, VZA
 156 dependencies, and variations in cloud microphysics. The small portions of the satellite pixel
 157 sampled by the narrow lidar footprint can cause some significant differences if the cloud height
 158 varies within the pixel. Errors in the temperature profiles can move Z_{eff} up or down. For example,
 159 some of the Z_{eff} values between 6 and 14 km in Figure 2a are lower than the corresponding
 160 values of Z_{topCAL} and account for ~ 1 km of the range in ΔZ . It could also account for some of the
 161 extreme overestimates. This type of error is likely to occur some of the time given that
 162 temperature profiles over much of the world are based on numerical weather analysis
 163 assimilation of temporally and spatially sparse observations. The VZA has little impact here.

164 To examine the impact of cloud microphysics on ΔZ , radiative transfer calculations were
 165 performed by applying the Discrete Ordinates Radiative Transfer (DISORT; *Stamnes et al.*
 166 [1988]) method to an example case. For a given layer, the layer thickness can be expressed as

167

$$168 \quad \Delta z_i = 4 \delta De \Delta \tau_i / 6 Q IWC_i, \quad (3)$$

169 where $\Delta\tau_i$ is the visible optical depth for cloud layer i , the visible extinction efficiency Q has a
170 value of ~ 2 , IWC_i is the layer ice water content, the density of ice is $\delta = 0.9 \text{ gm}^{-2}$, and D_{ei} is the
171 effective diameter of the ice crystals in the cloud layer.

172 The DISORT calculations assumed a cloud 7.0-km thick cloud with a top at 13 km in a
173 tropical atmosphere. The cloud was divided into 198 layers with layer thickness decreasing from
174 250 m at the base to 10 m at the top. The bottom-layer optical depth was specified at 12 to ensure
175 that the cloud is optically thick. Calculations were then performed to compute T_{eff} for a range of
176 IWC and three values of D_e . Uniform IWC was assumed for all layers above the base layer. Z_{eff}
177 was determined from T_{eff} and the simulated cloud-top height correction was computed as 13 km
178 $-Z_{eff}$. The optical depth of the layer above the cloud is the sum of the layer optical depths above
179 Z_{eff} . Assuming that approximately 1.5 km of the range in ΔZ (Figure 2a) is due to inaccurate
180 temperature profiles, the observed range would then be ~ 4.5 km. That extreme value of ΔZ could
181 occur for very large values of D_e and $IWC = 0.01 \text{ gm}^{-3}$ (Figure 3c) or for smaller values of IWC
182 and D_e (Figure 3b), but is unlikely to be observed for very small particles (Figure 3a). The
183 average bias at $Z_{eff} = 14$ km (Figure 1a) is 2.1 km, a value that can be explained, at $VZA = 14^\circ$,
184 with $IWC = 0.014 \text{ gm}^{-3}$ and $D_e = 80 \text{ }\mu\text{m}$, or with sets of smaller or larger values of IWC and D_e .
185 Although its value at 5 km is 62 μm , the observed mean D_e varies almost linearly from 55 μm at
186 $Z_{eff} = 6$ km to 76 μm at 12.6 km, then down to 64 μm at 15 km (not shown). At 14 km, $D_e \sim 68$
187 μm , which would correspond to $IWC \sim 0.011 \text{ gm}^{-3}$. At $Z_{eff} = 9$ km, $\Delta Z = 1.6$ km and $D_e = 68 \text{ }\mu\text{m}$,
188 corresponding to $IWC = 0.019 \text{ gm}^{-3}$. Since the optical depth corresponding to ΔZ is relatively
189 constant (Figure 3d), IWC can be estimated at each altitude using the proportional relationship

190

191
$$IWC = k D_e / \Delta Z, \quad (4)$$

192 where ΔZ is determined from Eq (1), D_e is the mean at Z_{eff} , and the proportionality constant k
193 was determined from Eq (4) to be 0.000334 gm^{-3} , based on the above estimate of IWC for $Z_{eff} =$
194 14 km and $D_e = 68 \text{ }\mu\text{m}$. Values of IWC were estimated for $Z_{eff} = 5 - 15 \text{ km}$ and fitted using a
195 third order polynomial regression to obtain

196

$$197 \quad \text{IWC} = 0.018 \text{ gm}^{-3} - 0.000474 Z_{eff}, \quad (5)$$

198

199 where Z_{eff} is in units of km. The squared linear correlation coefficient is 0.77 indicating that the
200 average IWC is a strong function of the cloud height. This fit does not apply to altitudes below 5
201 km. The range in mean IWC then is roughly between 0.01 and 0.02 gm^{-3} .

202 This result is not surprising given that the IWC has been observed to decrease with
203 decreasing cloud temperature. (T_{eff} was not used as the independent variable for the correction
204 developed here because the height differences were more highly correlated with Z_{eff} than with
205 T_{eff} .) *Heymsfield and Platt* [1984] reported that the mean IWC in cirrus clouds varied from 0.027
206 gm^{-3} at $T = -25^\circ\text{C}$ to 0.001 gm^{-3} at -58°C . They found that IWC variability for a given
207 temperature was typically an order of magnitude or greater. *Wang and Sassen* [2002] found that
208 IWC ranged from 0.017 to 0.001 gm^{-3} between -20 and -70°C for comparable clouds. *Garrett et*
209 *al.* [2005] observed IWC values as large as 0.3 gm^{-3} in a thick anvil cloud, while smaller values,
210 ranging from 0.0001 to 0.02 gm^{-3} , were observed by *McFarquhar and Heymsfield* [1996] in the
211 top 2 km of three tropical anvils. The mean IWC values estimated here for the top portions of
212 thick ice clouds over the non-polar globe are well within the range of observations. The variation
213 in the observed IWC's can also explain much of the random error seen in Figure 1b.

214 Figure 3e shows that the optical depth of the cloud layer above Z_{eff} is constant at ~ 1.15
 215 for $D_e = 80 \mu\text{m}$ increasing only slightly for tiny values of ΔZ (large IWC). It increases up to 1.5
 216 for $D_e = 10 \mu\text{m}$ (Figure 3d) and drops to smaller values for $D_e = 180 \mu\text{m}$ when $\Delta Z > 2.5 \text{ km}$
 217 (Figure 3f). The value of τ for the larger particles is slightly greater than that used by *Sherwood*
 218 *et al.* [2004] to estimate where the value of Z_{eff} should be in relation to the lidar observed top for
 219 convective anvils. The difference is mostly due to scattering. Based on the lidar-derived optical
 220 depths, *Sherwood et al.* [2004] concluded that the large values of ΔZ , which are similar to those
 221 in Figure 1a, did not correspond to $\tau = 1$, but to $\tau \geq 10$. Given the above analysis and the observed
 222 range of IWC in ice clouds, it appears that an average value of 2 km for ΔZ is quite reasonable
 223 and corresponds to $\tau \sim 1$ for the size of ice crystals retrieved with the VISST. For the matched
 224 CALIPSO-CERES data used here, the height where the CALIPSO beam was fully attenuated
 225 was, on average, 1.3 km below Z_{eff} , a value much greater than the 150 m calculated for a similar
 226 quantity based on the penetration depth of the airborne lidar used in the *Sherwood et al.* [2004]
 227 analysis. It is not clear why that earlier analysis produced such different results from the current
 228 analysis, but perhaps, may be due to assumptions used in the optical depth retrievals from the
 229 airborne lidar or differences in power between it and the CALIOP. Nevertheless, the current
 230 results are consistent with the expected values of IWC in the tops of ice clouds.

231 The optical depths in Figure 3 decrease with VZA as expected. While the small range in
 232 VZA for the current results precludes the development of an empirical correction for VZA
 233 dependence, however, the results in Figure 3 suggest that the dependence is a simple cosine
 234 variation. Thus, if $Z_{top}' = Z_{top}$ in either Eq (1) or (2), the VZA-corrected estimate of Z_{top} is

$$235 \quad Z_{top} = Z_{eff} + \Delta Z, \quad (6)$$

237 where $\Delta Z = \mu (Z_{top}' - Z_{eff})$. Validating the accuracy of Eq (6) will require a comprehensive
238 combined imager-lidar dataset having a wide range of VZAs.

239

240 **5. Concluding Remarks**

241 The effective radiating height of a cloud, as characterized by Z_{eff} , may be adequate for
242 radiative transfer calculations in climate or weather models, but the physical boundaries of a
243 cloud are needed by models to determine the layers where condensates form and persist. The
244 upper boundary is inadequately represented by Z_{eff} for ice clouds. This paper has developed a
245 simple parameterization that uses Z_{eff} to provide, on average, an unbiased estimate of Z_{top} for
246 optically thick ice clouds. This result complements the parameterizations used to estimate Z_{top} for
247 optically thin cirrus clouds. Much of the instantaneous uncertainty in the values of Z_{top}
248 determined with the new parameterization appears to be due to natural variations in the ice water
249 content near cloud top. Reducing the instantaneous uncertainty in Z_{top} may be possible using
250 combinations of different spectral channels or dual-angle views, but the reduction will be limited
251 by the accuracy of the temperature profile. When applied, the parameterization estimate of Z_{top}
252 should have the tropopause as an upper limit to minimize unrealistic results. Furthermore, it
253 should not be applied to low-level clouds; the selection of a minimum altitude will require
254 further study. Although this new parameterization of Z_{top} has been formulated in terms of Z_{eff}
255 determined from the 11- μm brightness temperature, it is probably applicable to Z_{eff} determined
256 using other infrared techniques such as CO₂ slicing. Although CALIPSO data from only 1 month
257 of orbits was used here, the results should be similar in other seasons. Testing with data from
258 other months would be required to confirm that contention and data from other satellites, that are

259 not near the CALIPSO ground track, would be needed to verify the formulation for off-nadir
260 angles.

261

262 **Acknowledgments**

263 This research was supported by NASA through the NASA Energy and Water Cycle Studies
264 Program and the CALIPSO and CERES Projects.

265 **References**

- 266 Dong, X., P. Minnis, B. Xi, S. Sun-Mack, and Y. Chen (2008), Comparison of CERES-MODIS
267 stratus cloud properties with ground-based measurements at the DOE ARM Southern Great
268 Plains site, *J. Geophys. Res.*, *113*, D03204, doi:10.1029/2007JD008438.
- 269 Heymsfield, A. and C. M. R. Platt (1984), A parameterization of the particle size spectrum of ice
270 clouds in terms of the ambient temperature and the ice water content, *J. Atmos. Sci.*, *41*, 846-
271 855.
- 272 McFarquhar, G. M. and A. J. Heymsfield (1996), Microphysical characteristics of three anvils
273 sampled during the Central Equatorial Pacific Experiment, *J. Atmos. Sci.*, *53*, 2401-2423.
- 274 Minnis, P., D. P. Garber, D. F. Young, R. F. Arduini, and Y. Takano (1998), Parameterizations
275 of reflectance and effective emittance for satellite remote sensing of cloud properties, *J.*
276 *Atmos. Sci.*, *55*, 3313-3339.
- 277 Minnis, P., and Co-authors (2006), Overview of CERES cloud properties from VIRS and
278 MODIS, *Proc. AMS 12th Conf. Atmos. Radiation*, Madison, WI, July 10-14, CD-ROM, J2.3.
- 279 Minnis, P., P. W. Heck, and E. F. Harrison (1990), The 27-28 October 1986 FIRE IFO cirrus
280 case study: cloud parameter fields derived from satellite data, *Mon. Weather Rev.*, *118*, 2426-
281 2447.
- 282 Minnis, P., and Co-authors (1995), Clouds and the Earth's Radiant Energy System (CERES)
283 algorithm theoretical basis document, volume III: Cloud analyses and radiance inversions
284 (subsystem 4), in *Cloud Optical Property Retrieval (Subsystem 4.3)*, vol. 3, *Rep. 1376*, edited
285 by the CERES Science Team, pp. 135-176, NASA, Hampton, Virginia.
- 286 Rossow, W. B. and R. A. Schiffer (1999), Advances in understanding clouds from ISCCP, *Bull.*
287 *Amer. Meteor. Soc.*, *80*, 2261-2287.

288 Sherwood, S. C., J.-H. Chae, P. Minnis, and M. McGill (2004), Underestimation of deep
289 convective cloud tops by thermal imagery, *Geophys. Res. Lett.*, *31*, L11102,
290 doi:10.1029/2004GL019699.

291 Stamnes, K., S. C. Tsay, W. Wiscombe and K. Jayaweera (1988), Numerically stable algorithm
292 for discrete-ordinate-method radiative transfer in multiple scattering and emitting layered
293 media, *Appl. Opt.*, *27*, 2502–2509.

294 Sun-Mack, S., B. A. Wielicki, P. Minnis, S. Gibson, and Y. Chen, 2007: Integrated cloud-
295 aerosol-radiation product using CERES, MODIS, CALISPO, and CloudSat data. *Proc. SPIE*
296 *Europe 2007 Conf. Remote Sens. Clouds and the Atmos.*, Florence, Italy, 17-19 September,
297 6745, no. 29.

298 Vaughan, M., Young, S., Winker, D., Powell, K., Omar, A., Liu, Z., Hu, Y., and Hostetler, C.
299 (2004), Fully automated analysis of space-based lidar data: an overview of the CALIPSO
300 retrieval algorithms and data products, *Proc. SPIE*, 5575, pp. 16-30.

301 Wang, Z. and K. Sassen (2002), Cirrus cloud microphysical property retrieval using lidar and
302 radar measurements. Part II: Midlatitude cirrus microphysical and radiative properties, *J.*
303 *Atmos. Sci.*, *59*, 2291-2302.

304 Winker, D. M., W. H. Hunt, and M. J. McGill (2007), Initial performance assessment of
305 CALIOP, *Geophys. Res. Lett.*, *34*, L19803, doi:10.1029/2007GL03135.

306

306 **Figure Captions**

307

308 **Figure 1.** CALIPSO products for 27 April 2007 over South Pacific, Antarctica, and southern
309 Indian Ocean. (a) CALIOP backscatter intensities, (b) CALIPSO feature mask with overlaid
310 CERES Aqua MODIS cloud top heights for optically thick ice clouds, (c) same as (b) except
311 with CERES cloud-top heights corrected with Eq (1).

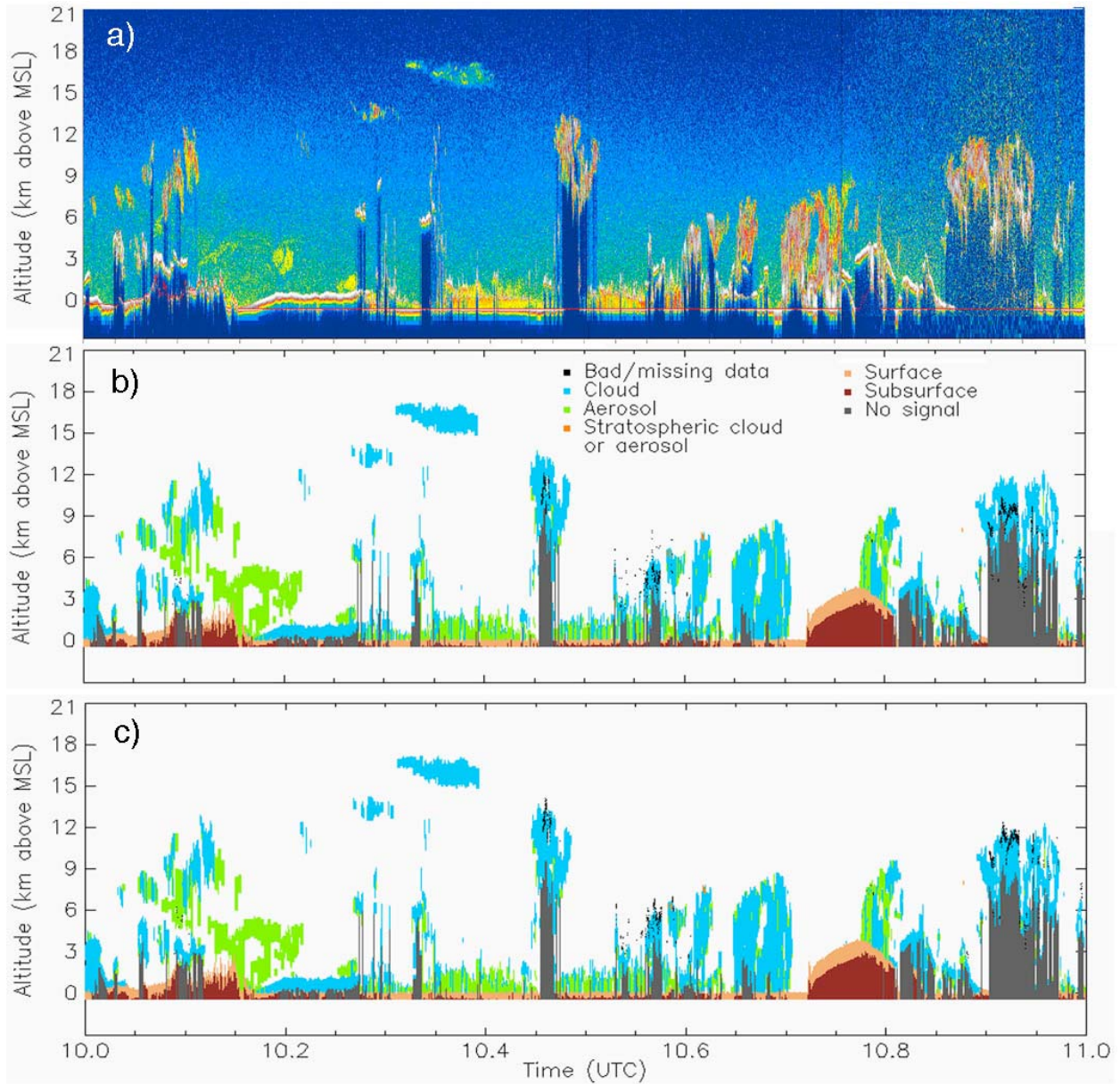
312

313 **Figure 2.** Scatter plots of CALIPSO optically thick non-polar cloud top altitudes during April
314 2007 versus (a) Z_{eff} for even days and (b) Z_{top} computed from Z_{eff} using Eq (1) for odd days.

315

316 **Figure 3.** Theoretical variation of (a-c) cloud-top/effective height difference (ΔZ) as function of
317 IWC for three ice crystal sizes and (d-f) optical depth of cloud layer above the effective radiating
318 height as function of ΔZ . Results are from DISORT calculations for a tropical atmosphere.

319



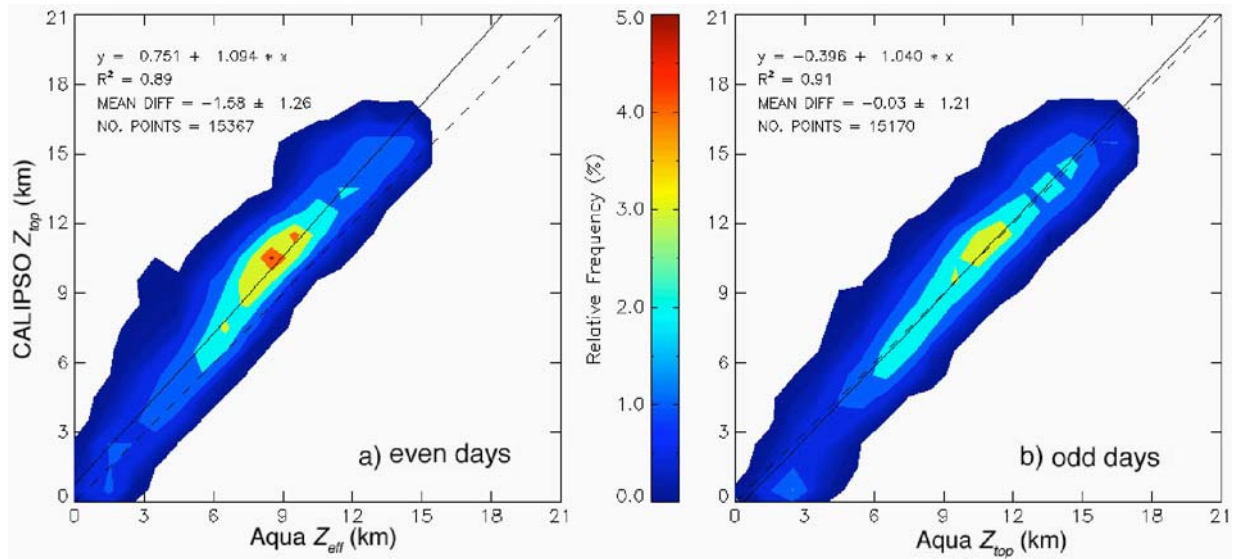
320

321 **Figure 1.** CALIPSO products for 27 April 2007. (a) CALIOP backscatter intensities, (b)

322 CALIPSO feature mask with overlaid CERES Aqua MODIS cloud top heights for optically thick

323 ice clouds, (c) same as (b) except with CERES cloud-top heights corrected with Eq (1).

324

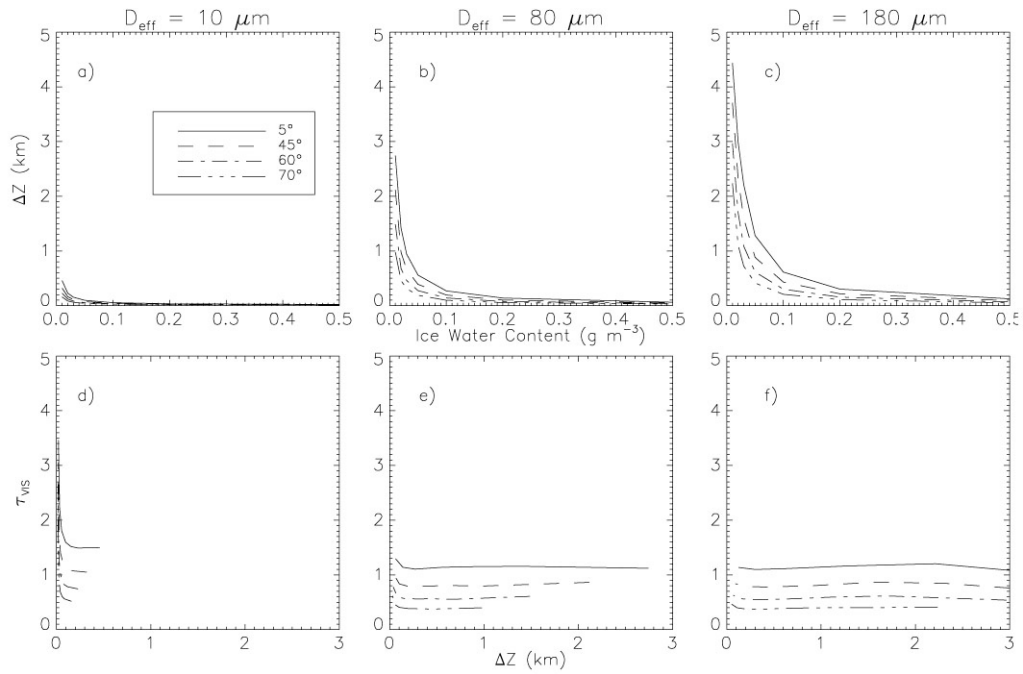


324

325 **Figure 2.** Scatter plots of CALIPSO optically thick non-polar cloud top altitudes during April

326 2007 versus (a) Z_{eff} for even days and (b) Z_{top} computed from Z_{eff} using Eq (1) for odd days.

327



327

328 **Figure 3.** Theoretical variation of (a-c) cloud-top/effective height difference (ΔZ) as function of
 329 IWC for three ice crystal sizes and (d-f) optical depth of cloud layer above the effective radiating
 330 height as function of ΔZ . Results are from DISORT calculations for a tropical atmosphere.

331